Hybrid Finite-Difference/Finite-Volume Time-Domain Analysis for Microwave Integrated Circuits with Curved PEC Surfaces Using a Nonuniform Rectangular Grid

Mingwu Yang, Yinchao Chen, *Member, IEEE*, and Raj Mittra, *Life Fellow, IEEE*

***Abstract*—In this paper, we present a hybrid algorithm that combines the finite-difference time-domain (FDTD) and finite-volume time-domain (FVTD) methods to analyze microwave integrated-circuit structures that may contain curved perfect electric conductor (PEC) surfaces. We employ the conventional nonuniform FDTD in regions where the objects are describable with a rectangular mesh, while applying the FVTD method elsewhere where we need to deal with curved PEC configurations. Both the FDTD and FVTD quantities are defined in the mutually overlapping regions, and these fields from the respective regions are interpolated by using their nearest neighbors. We validate this algorithm by analyzing the scattering parameters of a stripline with one or more adjacent cylindrical vias, whose geometries are frequently encountered in printed-circuit-board designs. It is found that the hybrid FDTD–FVTD approach requires little increase in central processing unit time and memory in comparison to the conventional FDTD, while its computational accuracy is significantly improved over a wide range of frequencies. Specifically, this accuracy is found to be comparable to that achieved by doubling the mesh density of the staircased FDTD.**

***Index Terms*—Hybrid FDTD–FVTD algorithm, microwave integrated circuits.**

I. Introduction

ONE OF THE most significant drawbacks of the conventional finite-difference time-domain (FDTD) method [1]–[3] is its inability to accurately model curved surfaces that are frequently encountered in practical electromagnetic problems, whose geometries are approximated by using a staircasing approach. Previous attempts to overcome this difficulty and to reduce the effect of discretization error have resulted in the development of various modified versions of the FDTD, e.g., FDTD on a curvilinear grid, contour-path integral FDTD [4], hybrid FDTD–finite-volume time-domain (FVTD) [5]–[8], and hybrid FDTD–finite-element time-domain (FETD) techniques [9]. In the conventional hybrid FDTD–FVTD approach [6]–[8], a geometrically conformal grid is required to construct the field solution, one that ensures that each cell is homogeneously filled with the same material. A great deal of effort is often required to generate a complex mesh that satisfies the above criterion.

In this paper, we present a hybridization scheme for combining the FDTD–FVTD algorithms, both operating on a nonuniform rectangular grid, to analyze microwave integrated circuits (MIC's) with curved surfaces that are perfect electric conductors (PEC's). Our primary objective is to retain the simplicity of the rectangular grid generation and still maintain the ability to handle curved PEC surfaces accurately, even when the object being analyzed is inhomogeneous. We accomplish this by using the FDTD in regions where the object is describable with a rectangular mesh, and switch to the FVTD in the complementary regions where its PEC surfaces are curved. For the cells that contain a combination of PEC and dielectric materials, we use an effective volume factor to modify the coefficients defined in the update FVTD equations. We retain a few overlapping layers between the FDTD and FVTD regions for the purpose of achieving a smooth transition of the fields from one region to the other via field interpolations. It is found that the hybrid FDTD–FVTD approach requires little increase in central processing unit (CPU) time and memory over the conventional FDTD. However, its computational accuracy is significantly improved, and is comparable to that achieved by using a staircased FDTD with twice the mesh density.

II. Hybridization of FDTD and FVTD

A. Nonuniform Orthogonal FDTD Algorithm

As mentioned earlier, we apply a nonuniform and orthogonal version of the FDTD Maxwell solver in regions that contain only rectangular-shaped objects, by using an algorithm that is similar to the ones described in [10] and [11]. The fundamental computational block is a pair of coupled FDTD cells, i.e., E- and H-cells, whose topology is illustrated in Fig. 1(a). Typical update equations, for instance, for the two x-components of the

Manuscript received June 10, 1998.

M. Yang is with the Department of Electronic and Information Engineering, Hong Kong Polytechnic University, Hong Kong.

Y. Chen was with the Department of Electronic and Information Engineering, Hong Kong Polytechnic University, Hong Kong. He is now with the Department of Electrical and Computer Engineering, University of South Carolina, Columbia, SC 29208 USA.

R. Mittra is with the EMC Research Laboratory, Pennsylvania State University, University Park, PA 16802 USA.

Publisher Item Identifier S 0018-9480(00)04659-7.

electric and magnetic fields, are given by (1) and (2), shown at the bottom of this page, with

$$a_e^x(i-1/2,\ j,\ k) = \frac{1-\dfrac{\sigma_x(i-1/2,\ j,\ k)\Delta t}{2\varepsilon_0\varepsilon_x(i-1/2,\ j,\ k)}}{1+\dfrac{\sigma_x(i-1/2,\ j,\ k)\Delta t}{2\varepsilon_0\varepsilon_x(i-1/2,\ j,\ k)}} \tag{3a}$$

$$b_e^x(i-1/2,\ j,\ k) = \frac{\dfrac{\Delta t}{\varepsilon_0\varepsilon_x(i-1/2,\ j,\ k)}}{1+\dfrac{\sigma_x(i-1/2,\ j,\ k)\Delta t}{2\varepsilon_0\varepsilon_x(i-1/2,\ j,\ k)}} \tag{3b}$$

$$c_h^x(i,\ j-1/2,\ k-1/2) = \frac{\Delta t}{\mu_0\mu_x(i,\ j-1/2,\ k-1/2)} \tag{3c}$$

$$\Delta y_e(j) = y(j) - y(j-1) \tag{4a}$$

$$\Delta z_e(k) = z(k) - y(k-1) \tag{4b}$$

$$\Delta y_h(j) = \big[y(j+1) - y(j-1)\big]/2 \tag{4c}$$

$$\Delta z_h(k) = \big[z(k+1) - z(k-1)\big]/2 \tag{4d}$$

where $\Delta y_{e,\,h}(j)$ and $\Delta z_{e,\,h}(k)$ are nonuniform edge lengths for the E- and H-cells, respectively. For the sake of generality, we assume that all the medium parameters are characterized by a biaxial tensor form.

B. Nonuniform Orthogonal FVTD Algorithm

Next, we turn to the problem of updating the field quantities in regions that involve curved PEC surfaces. In contrast to the conventional FVTD, which is based on a geometry-conformal grid [5]–[8], the present version retains the use of a nonuniform rectangular grid. Fig. 1(b) shows the basic topology of the stencil, i.e., a pair of coupled E- and H-cells. We let the electric field reside at the center of the E-cell and locate the eight magnetic vectors at the eight vertices of this cell—and *vice versa* for the

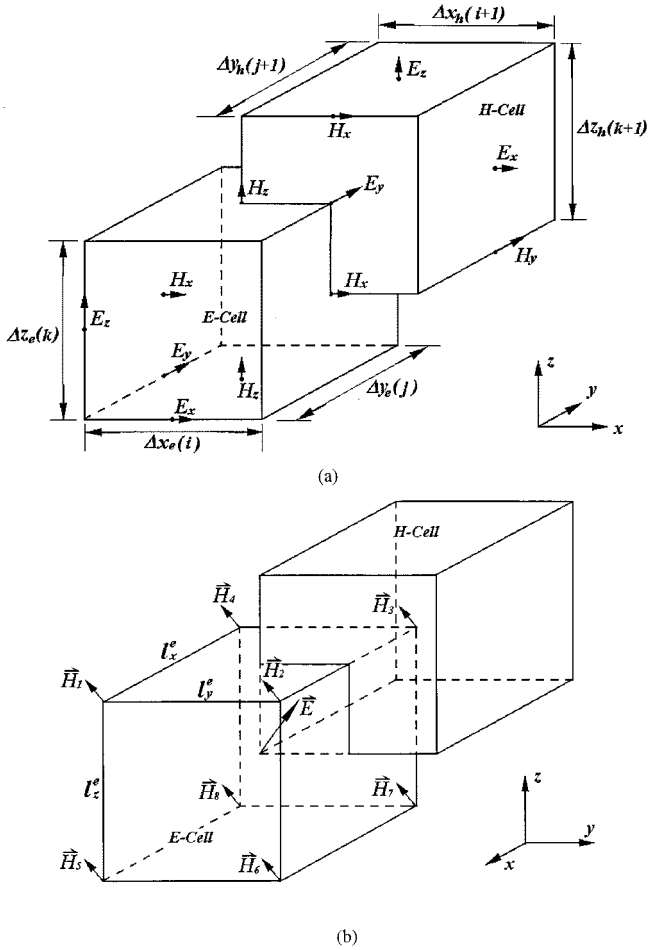

Fig. 1. Topology of the dual FDTD and FVTD cells based on a nonuniform rectangular grid: (a) FDTD. (b) FVTD.

$$E_x^{n+1}(i-1/2,\ j,\ k) = a_e^x(i-1/2,\ j,\ k)E_x^n(i-1/2,\ j,\ k) + b_e^x(i-1/2,\ j,\ k) \cdot \left[\begin{array}{l} \dfrac{H_z^{n+1/2}(i-1/2,\ j+1/2,\ k) - H_z^{n+1/2}(i-1/2,\ j-1/2,\ k)}{\Delta y_h(j)} \\ -\dfrac{H_y^{n+1/2}(i-1/2,\ j,\ k+1/2) - H_y^{n+1/2}(i-1/2,\ j,\ k-1/2)}{\Delta z_h(k)} \end{array}\right] \tag{1}$$

$$H_x^{n+1/2}(i,\ j-1/2,\ k-1/2) = H_x^{n-1/2}(i,\ j-1/2,\ k-1/2) - c_h^x(i,\ j-1/2,\ k-1/2) \cdot \left[\begin{array}{l} \dfrac{E_z^n(i,\ j,\ k-1/2) - E_z^n(i,\ j-1,\ k-1/2)}{\Delta y_e(j)} \\ -\dfrac{E_y^n(i,\ j-1/2,\ k) - E_y^n(i,\ j-1/2,\ k-1)}{\Delta z_e(k)} \end{array}\right] \tag{2}$$

H-cells. Integrating the two Maxwell's curl equations over an arbitrary volume (V) leads to the following:

$$\frac{\partial}{\partial t}\iiint_V \varepsilon\vec{E}\,dV + \iiint_V \sigma\vec{E}\,dV = \oiint_s d\vec{S}\times\vec{H} \tag{5a}$$

$$\frac{\partial}{\partial t}\iiint_V \mu\vec{H}\,dV = -\oiint_s d\vec{S}\times\vec{E}. \tag{5b}$$

Implementing the above relations in, say, the $(i,\ j,\ k)$th coupled E- and H-FVTD cells, we can derive a leapfrog FVTD update equation as follows:

$$E_P^{n+1}(i,\ j,\ k) = \alpha_P(i,\ j,\ k)E_P^n(i,\ j,\ k) + \beta_P(i,\ j,\ k)Q_P^{n+1/2}(i,\ j,\ k) \tag{6a}$$

$$H_P^{n+1/2}(i,\ j,\ k) = H_P^{n-1/2}(i,\ j,\ k) - \gamma_P(i,\ j,\ k)S_P^n(i,\ j,\ k) \tag{6b}$$

where $P = x$, y, or z, and the time-domain electric and magnetic fields are defined at the centers of the $(i,\ j,\ k)$th E and H-cells, respectively. The remaining parameters in (6) are given by

$$\alpha_P(i,\ j,\ k) = \frac{1-\dfrac{\sigma_P(i,\ j,\ k)\Delta t}{2\varepsilon_0\varepsilon_P(i,\ j,\ k)}}{1+\dfrac{\sigma_P(i,\ j,\ k)\Delta t}{2\varepsilon_0\varepsilon_P(i,\ j,\ k)}} \tag{7a}$$

$$\beta_P(i,\ j,\ k) = \frac{2\Delta t}{l_x^e(i)l_y^e(j)l_z^e(k)\left[2\varepsilon_0\varepsilon_P(i,\ j,\ k)+\Delta t\sigma_P(i,\ j,\ k)\right]} \tag{7b}$$

$$\gamma_P(i,\ j,\ k) = \frac{\Delta t}{l_x^h(i)l_y^h(j)l_z^h(k)\mu_0\mu_P(i,\ j,\ k)} \tag{8}$$

and

$$\begin{aligned} Q_x^{n+1/2}(i,\ j,\ k) &= \frac{1}{4}l_z^e(k)l_x^e(i)\Big(H_{2z}^{n+1/2}+H_{3z}^{n+1/2}+H_{6z}^{n+1/2} \\ &\quad +H_{7z}^{n+1/2}-H_{1z}^{n+1/2}-H_{4z}^{n+1/2} \\ &\quad -H_{5z}^{n+1/2}-H_{8z}^{n+1/2}\Big) \\ &\quad -\frac{1}{4}l_y^e(j)l_x^e(i)\Big(H_{1y}^{n+1/2}+H_{2y}^{n+1/2}+H_{3y}^{n+1/2} \\ &\quad +H_{4y}^{n+1/2}-H_{5y}^{n+1/2}-H_{6y}^{n+1/2} \\ &\quad -H_{7y}^{n+1/2}-H_{8y}^{n+1/2}\Big) \end{aligned} \tag{9a}$$

$$\begin{aligned} Q_y^{n+1/2}(i,\ j,\ k) &= \frac{1}{4}l_x^e(i)l_y^e(j)\Big(H_{1x}^{n+1/2}+H_{2x}^{n+1/2}+H_{3x}^{n+1/2} \\ &\quad +H_{4x}^{n+1/2}-H_{5x}^{n+1/2}-H_{6x}^{n+1/2} \\ &\quad -H_{7x}^{n+1/2}-H_{8x}^{n+1/2}\Big) \\ &\quad -\frac{1}{4}l_z^e(k)l_y^e(j)\Big(H_{1z}^{n+1/2}+H_{2z}^{n+1/2}+H_{5z}^{n+1/2} \\ &\quad +H_{6z}^{n+1/2}-H_{4z}^{n+1/2}-H_{3z}^{n+1/2} \\ &\quad -H_{8z}^{n+1/2}-H_{7z}^{n+1/2}\Big) \end{aligned} \tag{9b}$$

$$\begin{aligned} Q_z^{n+1/2}(i,\ j,\ k) &= \frac{1}{4}l_y^e(j)l_z^e(k)\Big(H_{1y}^{n+1/2}+H_{2y}^{n+1/2}+H_{5y}^{n+1/2} \\ &\quad +H_{6y}^{n+1/2}-H_{4y}^{n+1/2}-H_{3y}^{n+1/2} \\ &\quad -H_{8y}^{n+1/2}-H_{7y}^{n+1/2}\Big) \\ &\quad -\frac{1}{4}l_x^e(i)l_z^e(k)\Big(H_{2x}^{n+1/2}+H_{3x}^{n+1/2}+H_{6x}^{n+1/2} \\ &\quad +H_{7x}^{n+1/2}-H_{1x}^{n+1/2}-H_{4x}^{n+1/2} \\ &\quad -H_{5x}^{n+1/2}-H_{8x}^{n+1/2}\Big) \end{aligned} \tag{9c}$$

where the $l_P^{e,\,h}$ is the edge length of the (i,j,k)th E or H-cell in the P-direction. The eight magnetic fields surrounding the E-cell are located at the eight vertices, and they may be explicitly written as

$$\begin{aligned} \vec{H}_1 &= \vec{H}(i+1/2,\ j-1/2,\ k+1/2) \\ \vec{H}_2 &= \vec{H}(i+1/2,\ j+1/2,\ k+1/2) \end{aligned} \tag{10a}$$

$$\begin{aligned} \vec{H}_3 &= \vec{H}(i-1/2,\ j+1/2,\ k+1/2) \\ \vec{H}_4 &= \vec{H}(i-1/2,\ j-1/2,\ k+1/2) \end{aligned} \tag{10b}$$

$$\begin{aligned} \vec{H}_5 &= \vec{H}(i+1/2,\ j-1/2,\ k-1/2) \\ \vec{H}_6 &= \vec{H}(i+1/2,\ j+1/2,\ k-1/2) \end{aligned} \tag{10c}$$

$$\begin{aligned} \vec{H}_7 &= \vec{H}(i-1/2,\ j+1/2,\ k-1/2) \\ \vec{H}_8 &= \vec{H}(i-1/2,\ j-1/2,\ k-1/2). \end{aligned} \tag{10d}$$

Similarly, we can define the updated quantities $S_{x,\,y,\,z}^n(i,\ j,\ k)$ in the $(i,\ j,\ k)$th H-cell and its surrounding eight electric fields.

The cells containing the curved PEC surfaces can, in general, be inhomogeneous and contain two or more different materials. One consequence of this is that the coefficients in the update equation (6a) in an E-cell now become different. The following three situations can arise.

1) If an E-cell is a uniform homogeneous lossless dielectric, then the coefficient $\alpha_p(i,\ j,\ k) = 1$.
2) If an E-cell only has a PEC, then $\alpha_p(i,\ j,\ k) = \beta_p(i,\ j,\ k) = 0$.
3) If an E-cell is a combination of a lossless dielectric and a conductor, $\alpha_p(i,\ j,\ k)$ remains unity, but $\beta_p(i,\ j,\ k)$ must be weighted by an effective volume factor $V_{\rm eff}(i,\ j,\ k)$, defined as the ratio of the volume of lossless dielectric to the total volume of the E-cell, and the update (6a) becomes

$$E_P^{n+1}(i,\ j,\ k) = \alpha_P(i,\ j,\ k)E_P^n(i,\ j,\ k) + V_{\rm eff}(i,\ j,\ k)\cdot\beta_P(i,\ j,\ k)Q_P^{n+1/2}(i,\ j,\ k). \tag{11}$$

Note that this yields consistent results for the two limiting cases, i.e., $V_{\rm eff}(i,\ j,\ k) = 1$ for a cell filled with a uniform lossless dielectric, and zero for a PEC cell. In particular, the present technique does not require a PEC or an impedance boundary at a discontinuity interface between a dielectric and a PEC structure

inside an FVTD region, as does the conventional FVTD with a tetrahedron grid used to fit the curved PEC surfaces [8].

C. Interpolation in the FDTD–FVTD Overlapping Regions

Rather than using a more complex and generalized overlapping technique in the FDTD–FVTD overlapping region where the FDTD and FVTD grids are nonaligned [12], we employ an identical rectangular grid for both the FDTD and FVTD algorithms in the overlapping region. One consequence of this is that the interpolations between the FDTD and FVTD field quantities can be carried out relatively easily. As shown in Fig. 1, the center of the $(i,\ j,\ k)$th FVTD E-cell is located at the node $(i,\ j,\ k)$, where the three components of FVTD electric fields are defined, while the three components of the FDTD electric fields in the $(i,\ j,\ k)$th cell are located at $(i-1/2,\ j,\ k)$, $(i,\ j-1/2,\ k)$, $(i,\ j,\ k-1/2)$, respectively. We define an overlapping layer between the FDTD and FVTD regions for interpolating the FDTD and FVTD fields. We now present two interpolation techniques that have been found to provide the smoothest transition of time-domain fields from one region to the other.

1) Interpolation Over an FDTD–FVTD Overlapping Layer with a Finite Thickness: The first choice for handing the transition region between the FDTD and FVTD is to employ an overlapping region with a finite layer thickness. For this case, the electric fields on the outer boundary of the FVTD, e.g., $\vec{E}^v$, can be linearly interpolated by using the nearest FDTD fields, E^D_{1P} and E^D_{2P}, as shown in Fig. 2(a), to yield

$$E^V_P = \frac{l_{P2}E^D_{1P} + l_{P1}E^D_{2P}}{l_{P1} + l_{P2}} \tag{12a}$$

where $P = x,\ y,\ z$. For instance, the y-component of the $\vec{E}^v$ can be calculated from

$$E^V_y = \frac{l_{y2}E^D_{1y} + l_{y1}E^D_{2y}}{l_{y1} + l_{y2}}. \tag{12b}$$

At the inner boundary of the FDTD, which is inside the FVTD region, the FDTD tangential electric field E^D_t can also be linearly interpolated by using the nearest fields of the FVTD as follows:

$$E^D_t = \frac{E^V_{1t} + E^V_{2t}}{2} \tag{13}$$

where t designates the tangential components of the fields. Although the above method is relatively straightforward to implement, it does require additional computer storage for the fields in the overlapping region.

2) Interpolation Over an Infinitesimally Thin FDTD–FVTD Interface: An alternative to the approach just described above is to choose the FDTD–FVTD overlapping region as an infinitesimally thin interface. In this case the tangential FDTD electric fields on the interface, i.e., E^D_{1x} and E^D_{2x} [see Fig. 2(b)], are still determined with the conventional FDTD updating procedure by using the four surrounding magnetic fields, respectively. However, one of the magnetic fields is now located in the FVTD region; hence, it must first be interpolated by using the nearest FVTD magnetic fields. For example, an FVTD electric field, i.e., $\vec{E}^V_1$, on the interface can be interpolated by using

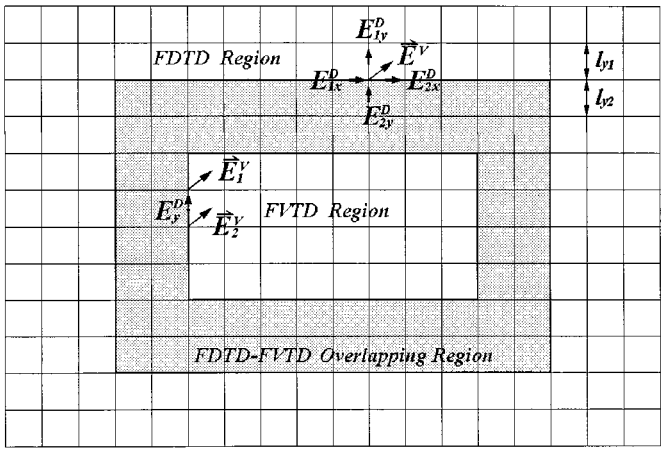

(a)

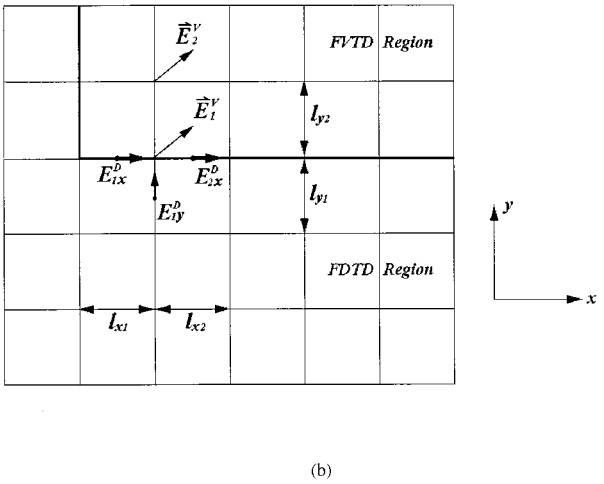

(b)

Fig. 2. Interpolation techniques within an FDTD–FVTD overlapping layer (a) Layer with thickness. (b) Infinitesimally thin interface.

$(E^D_{1x},\ E^D_{2x})$ and $(E^D_{1y},\ E^V_{2y})$ for its tangential and normal components, respectively, to yield

$$E^V_{1x} = \frac{l_{x2}E^D_{1x} + l_{x1}E^D_{2x}}{l_{x1} + l_{x2}} \tag{14a}$$

$$E^V_{1y} = \frac{2l_{y2}E^D_{1y} + l_{y1}E^V_{2y}}{l_{y1} + 2l_{y2}}. \tag{14b}$$

The above scheme requires no additional memory, and yet it turns out to be a simple, efficient, and accurate technique for interpolating the fields. In particular, it has been found that this interpolation scheme presents the same high level of accuracy as the previous one in this analysis. In addition, the two interpolation methods share the same level of excellent stability; hence, in practice, we only employ the second interpolation scheme, which requires no overlapping layer.

III. Numerical Results

To validate the hybrid FDTD–FVTD algorithm, we analyze a stripline with one or more cylindrical vias, a geometry that is frequently encountered in an integrated printed circuit board (PCB). The front and top views of the geometry are displayed

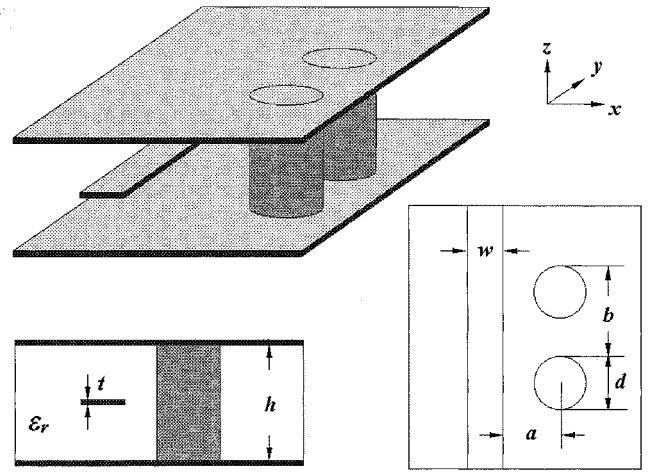

Fig. 3. Geometry of a stripline with two adjacent cylindrical vias.

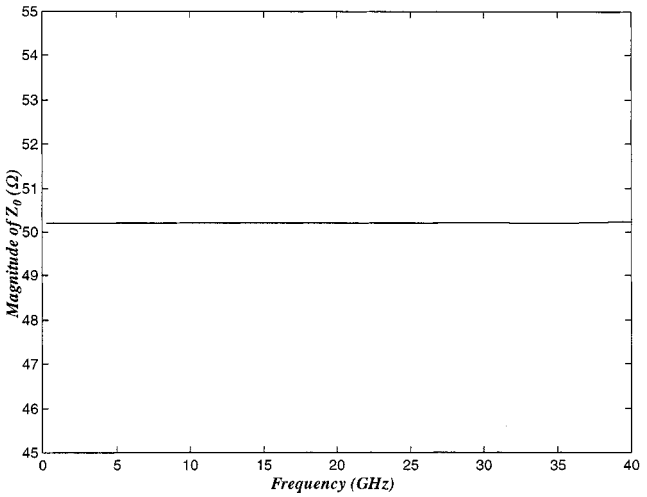

Fig. 4. Magnitude of characteristic impedance Z_0 as a function of frequency for a uniform strip line ($h = 1.2, w = 0.6, t = 0.1$ mm; $\varepsilon_r = 2.62$) calculated with the FDTD and hybrid approaches, respectively.

in Fig. 3. We excite the structure symmetrically with a Gaussian pulse, at the lower and upper sides of the strip, with an E_z component of the field, and apply a second-order dispersive absorbing condition for mesh truncation [13].

As a preamble to addressing the via problem, we investigate the characteristic impedance Z_0 of a uniform stripline by using both the FDTD and hybrid FDTD–FVTD approaches , as shown in Fig. 4. We find that both the magnitude and phase of the Z_0, obtained by using the FDTD and the hybrid approach, are essentially identical for this canonical test problem. However, this helps us to set the stage for the follow-up step, in which the computational domain, which is designated here as the FVTD region, is modified by the introduction of the vias. To see how the vias affect the propagation of the time-domain signals, we sample the normalized voltage signals at the input and output ports with and without a cylindrical via. It is found that a small ripple of time-domain voltage signal appears at the output port.

Next, we evaluate the accuracy of the hybrid algorithm by analyzing the scattering parameter S_{11} of a stripline with vias. The following three cases have been investigated:

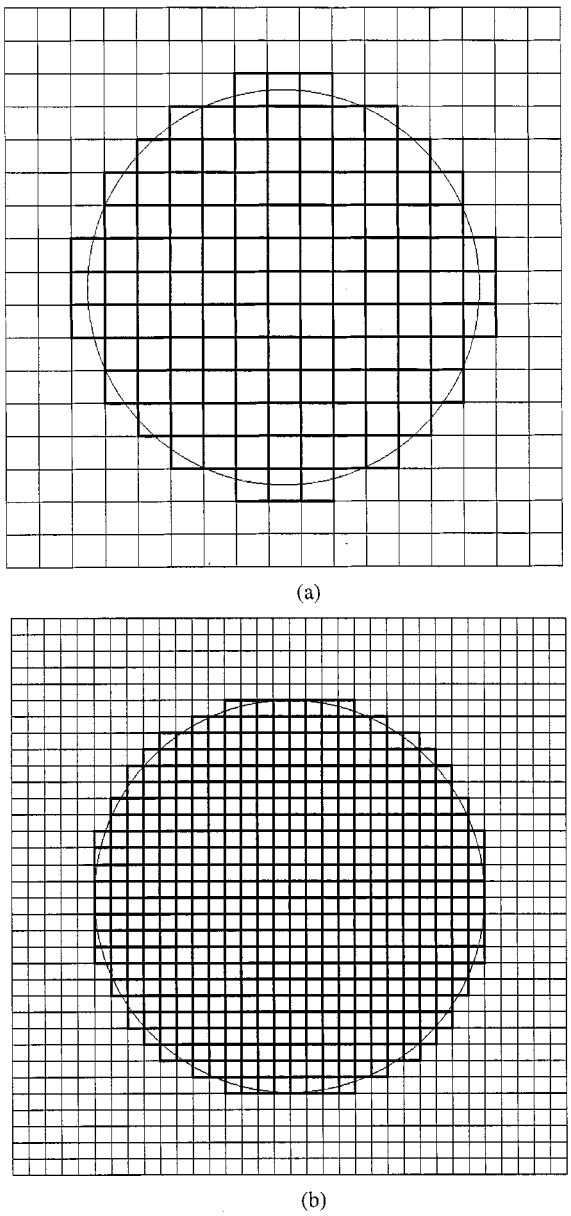

Fig. 5. Top view of mesh patterns around a via. (a) Coarse-mesh density ($\Delta x = \Delta y = 0.1$, $\Delta z = 0.11$ mm). (b) Double-mesh density ($\Delta x = \Delta y = 0.05$, $\Delta z = 0.11$ mm).

1) staircased FDTD approach on a coarse mesh ($\Delta x = \Delta y = 0.1$, $\Delta z = 0.11$ mm);
2) hybrid method also applied on a coarse mesh;
3) staircased FDTD approach with a mesh size given by $\Delta x = \Delta y = 0.05$, $\Delta z = 0.11$ mm, which is finer by a factor of two in the x- and y-directions than it is in the z-direction.

The region containing the cylindrical vias is chosen to be the FVTD region. The mesh patterns for the coarse- and fine-mesh densities at the cross section of one of the vias are displayed in Fig. 5(a) and (b). It is evident from Fig. 6(a) and (b) that the computational accuracy achieved by using the hybrid approach is comparable to that obtained by doubling the mesh density in the conventional FDTD method that exacts a significant increase in cost in terms of CPU time and memory. Note that all the results

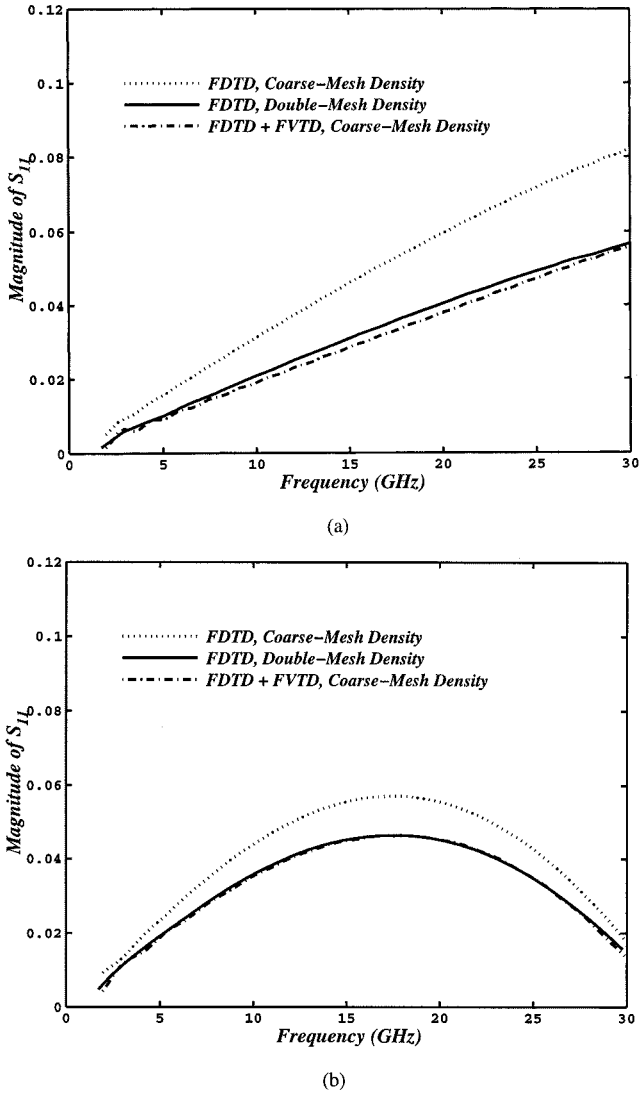

Fig. 6. Magnitude of scattering parameter S_{11} as a function of frequency for a stripline with adjacent vias ($h = 1.2$, $w = 0.6$, $t = 0.1$, $a = 1.55$ mm, $\varepsilon_r = 2.62$). (a) One via. (b) Two vias ($b = 1.44$ mm).

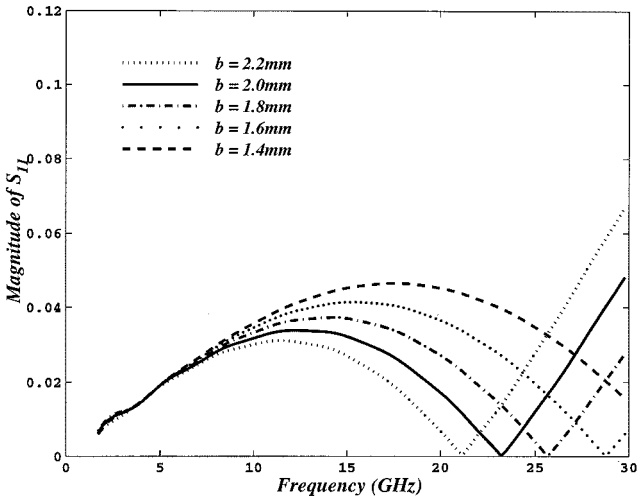

Fig. 7. Magnitude of scattering parameter S_{11} as a function of frequency for a stripline with two adjacent vias ($h = 1.2$, $w = 0.6$, $t = 0.1$, $d = 1.2$, $a = 1.55$ mm, $\varepsilon_r = 2.62$).

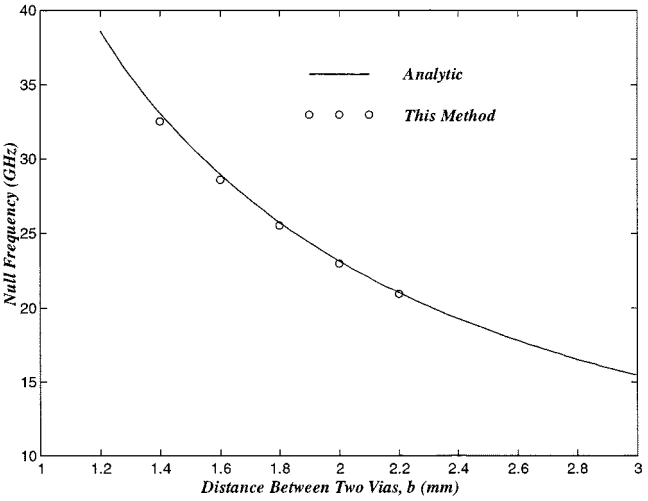

Fig. 8. Null frequency versus the distance b between two vias ($h = 0.6$, $t = 0.1$, $w = 0.6$, $s = 0.4$, $d = 0.6$, $a = 0.4$ mm).

derived from the hybrid FDTD–FVTD method have been obtained by using the infinitesimally thin interpolation scheme. It was found that the calculations remained stable for all the cases investigated in this paper, when the FDTD–FVTD overlapping regions are chosen appropriately. It is expected that the algorithm would also be useful for analyzing the resonant type of microwave structures when it is used in conjunction with extrapolation techniques [14], [15] to avoid any late time instability.

Before closing, we would like to make some observations regarding the influence of the via locations on the frequency behavior of the reflection coefficient. We note that the magnitude of the reflection coefficient for the one-via structure increases almost linearly as the operating frequency is increased, while the response of the two-via structure is considerably different, as it exhibits a dip from 20 to 30 GHz for different values of the distance b between the two vias (see Fig. 7). This is because the reflected waves from the two vias interfere destructively—when the phase difference between them approaches π at a particular frequency—to yield a reflection coefficient that is almost zero. In Fig. 7, we see that the null frequency where this occurs decreases monotonously with an increase in b. In fact, the null frequency can be predicted precisely from the out-of-phase condition, and is given by $f_{\text{null}} = V_P/(4b)$, where V_P is the phase velocity of the wave. In Fig. 8, we see that the null frequency predicted by using the above relation is in very good agreement with the computed one directly.

IV. Conclusions

In this paper, we have presented a hybrid FDTD–FVTD algorithm for the analysis of MIC's with curved PEC surfaces. The algorithm is based on the use of a nonuniform rectangular grid, and has been validated by analyzing the S-parameters of a stripline with two cylindrical vias that are close to each other. It is found that, for this structure, the hybrid approach significantly improves the computational accuracy, and yields results that are

comparable to those obtained by doubling the mesh density in the staircased-FDTD approach.

REFERENCES

[1] K. S. Yee, "Numerical solution of initial boundary value problems involving Maxwell's equations in isotropic media," *IEEE Trans. Antennas Propagat.*, vol. AP-14, pp. 302–307, May 1966.

[2] A. Taflove, *Computational Electrodynamics: The Finite Difference Time Domain Method*. Norwood, MA: Artech House, 1995.

[3] K. S. Kunz and R. J. Luebbers, *The Finite-Difference Time-Domain Method for Electromagnetics*. Boca Raton, FL: CRC Press, 1993.

[4] T. G. Jurgens, A. Taflove, K. Umashankar, and T. G. Moore, "Finite-difference time-domain modeling of curved surfaces," *IEEE Trans. Antennas Propagat.*, vol. 40, pp. 357–366, Apr. 1992.

[5] V. Shankar, A. H. Mohammadian, and W. F. Hall, "A time-domain, finite-volume treatment for the Maxwell equations," *Electromag.*, vol. 10, pp. 127–145, 1990.

[6] K. S. Yee and J. S. Chen, "The finite-difference time-domain (FDTD) and the finite-volume time-domain (FVTD) methods in solving Maxwell's equations," *IEEE Trans. Antennas Propagat.*, vol. 45, pp. 354–363, Mar. 1997.

[7] ——, "Conformal hybrid finite difference time domain and finite volume time domain," *IEEE Trans. Antennas Propagat.*, vol. 42, pp. 1450–1455, Oct. 1994.

[8] ——, "Impedance boundary condition simulation in the FDTD/FVTD hybrid," *IEEE Trans. Antennas Propagat.*, vol. 45, pp. 921–925, June 1997.

[9] D. Koh, H. Lee, and T. Itoh, "A hybrid full-wave analysis of via-hole grounds using finite-difference and finite-element time-domain methods," *IEEE Trans. Microwave Theory Tech.*, vol. 45, pp. 2217–2222, Dec. 1997.

[10] J. A. Svigelj, "Efficient solution of Maxwell's equations using the nonuniform orthogonal finite difference time domain method," Ph.D. dissertation, Dept. Elect. Comput. Eng., Univ. Illinois at Urbana-Champaign, Urbana-Champaign, IL, 1995.

[11] S. D. Gedney and F. Lansing, "Explicit time-domain solution of Maxwell's equation using nonorthogonal and unstructured grids," in *Computational Electrodynamics: The Finite Difference Time Domain Method*, A. Taflove, Ed. Norwood, MA: Artech House, 1995, ch. 11.

[12] K. S. Yee, J. S. Chen, and A. H. Chang, "Conformal finite-difference time-domain (FDTD) with overlapping grids," *IEEE Trans. Antennas Propagat.*, vol. 40, pp. 1068–1075, Sept. 1992.

[13] Z. Bi, K. Wu, C. Wu, and J. Litva, "A dispersive boundary condition for microstrip component analysis using the FDTD," *IEEE Trans. Microwave Theory Tech.*, vol. 40, pp. 774–777, Apr. 1992.

[14] W. L. Ko and R. Mittra, "A combination of FD-TD and Prony's methods for analyzing microwave integrated circuits," *IEEE Trans. Microwave Theory Tech.*, vol. 39, pp. 2176–2181, Dec. 1991.

[15] T. K. Sarkar and O. Pereira, "Using the matrix pencil method to estimate the parameters of a sum of complex exponentials," *IEEE Antennas Propagat. Mag.*, vol. 37, pp. 48–55, Feb. 1995.

Mingwu Yang received the B.Sc. and M.Sc. degrees from the Hefei University of Technology, Hefei, China, in 1982, and a joint program degree from the Anhui Institute of Optics and Fine Mechanics, Anhui, China, and the Chinese Academy of Sciences, Beijing, China, in 1988.

From 1988 to 1997, he was a Lecturer at the Hefei University of Technology, with a concentration in information optics and holography. He is currently a Research Assistant with the Department of Electronic and Information Engineering, Hong Kong Polytechnic University, Hong Kong, where he is engaged in numerical analysis for application of microwave integrated circuits and mobile antennas.

Yinchao Chen (M'94) received the Ph.D. degree in electrical engineering from the University of South Carolina, Columbia, in 1992.

During his earlier career in China, he was a Microwave and Antenna Engineer with the Nanjing Research Institute of Electronic Technology. From 1989 to 1995, he was a Teaching and Research Assistant, Post-Doctoral Fellow, Adjunct Assistant Professor, and Visiting Scholar Fellow with the University of South Carolina, South Carolina State University, and the University of Illinois at Urbana-Champaign, respectively. He was an Assistant Professor with the Department of Electronic and Information Engineering, Hong Kong Polytechnic University, Hong Kong, from October 1995 to June 2000. Since July 2000, he has been an Associate Professor with the Department of Electrical and Computer Engineering, University of South Carolina. His current research interests include computational electromagnetics with applications in the areas of millimeter-wave integrated circuits, wireless communication applications, electronic packaging modeling for VLSI devices, and microwave antenna applications. He has authored or co-authored over 80 international publications in refereed journals and conference symposiums.

Raj Mittra (S'54–M'57–SM'69–F'71–LF'96) is a Professor in the Electrical Engineering Department, Pennsylvania State University, University Park. He is also the Director of the Electromagnetic Communication Laboratory, which is affiliated with the Communication and Space Sciences Laboratory, Electrical Engineering Department. Prior to joining Pennsylvania State University, he was a Professor of electrical and computer engineering at the University of Illinois at Urbana-Champaign. He has been a Visiting Professor at Oxford University, Oxford, U.K., and at the Technical University of Denmark, Lyngby, Denmark. He is President of RM Associates, which is a consulting organization that provides services to industrial and governmental organizations, both in the U.S. and abroad. For the last 15 years, he has directed, as well as lectured in, numerous short courses on electronic packaging and computational electromagnetics, both nationally and internationally. He has authored or co-authored over 500 journal papers and 30 books or book chapters on various topics related to electromagnetics, antennas, microwaves, and electronic packaging. He holds three patents on communication antennas. His professional interests include the areas of RF circuit design, computational electromagnetics, electromagnetic modeling, and simulation of electronic packages, communication antenna design including global-positioning systems (GPS's), broad-band antennas, electromagnetic compatibility (EMC) analysis, radar scattering, frequency-selective surfaces, microwave and millimeter-wave integrated circuits, and satellite antennas. He currently serves as the North American Editor of *AEU*.

Dr. Mittra is Past–President of the IEEE Antennas and Propagation Society (IEEE AP-S). He has served as editor-in-chief of the IEEE TRANSACTIONS ON ANTENNAS AND PROPAGATION. He was the recipient of the 1965 Guggenheim Fellowship Award, the 1984 IEEE Centennial Medal, and the 2000 IEEE Millennium Medal.